Experimental Study of Thin Film Sensor Networks for Wind Turbine Blade Damage Detection

A. Downey[1,a)], S. Laflamme[1], F. Ubertini[2], H Sauder[3], and P. Sarkar[3]

[1]Department of Civil, Construction and Environmental Engineering, Iowa State University, USA
[2]Department of Civil and Environmental Engineering, University of Perugia, Italy
[3]Department of Aerospace Engineering, Iowa State University, USA.

[a)] adowney2@iastate.edu

Abstract. Damage detection of wind turbine blades is difficult due to their complex geometry and large size, for which large deployment of sensing systems is typically not economical. A solution is to develop and deploy dedicated sensor networks fabricated from inexpensive materials and electronics. The authors have recently developed a novel skin-type strain gauge for measuring strain over very large surfaces. The skin, a type of large-area electronics, is constituted from a network of soft elastomeric capacitors. The sensing system is analogous to a biological skin, where local strain can be monitored over a global area. In this paper, we propose the utilization of a dense network of soft elastomeric capacitors to detect, localize, and quantify damage on wind turbine blades. We also leverage mature off-the-shelf technologies, in particular resistive strain gauges, to augment such dense sensor network with high accuracy data at key locations, therefore constituting a hybrid dense sensor network. The proposed hybrid dense sensor network is installed inside a wind turbine blade model, and tested in a wind tunnel to simulate an operational environment. Results demonstrate the ability of the hybrid dense sensor network to detect, localize, and quantify damage.

INTRODUCTION

Implementation of a structural health monitoring (SHM) for wind turbine blades is difficult due to their complex geometry, large size and the high cost of traditional sensing systems [1]. Such large-scale components, along with other mesosystems including aerospace structures, energy systems and civil infrastructures are traditionally inspected and maintained via time-based or breakdown-based maintenance strategies. Automated damage detection, localization, and prognosis of structural systems or components may lead to strong economic benefits for owners, operators, and society. The deployment of condition-based maintenance (CBM) management has shown substantial economic benefits [2, 3, 4].

Cost effective monitoring solutions for mesoscale structures need to be capable of monitoring the structures' global (e.g., changing load paths, loss in global stiffness) and local (e.g., crack propagation) conditions. However, current sensing technologies and practices limit the distinction between localized and global faults on a mesoscale system [5, 6]. In the case of wind turbine blades, SHM is complicated further by the dependence of sensor signals on local environmental conditions such as temperature and humidity [7, 8]. A solution to the global/local condition monitoring problem is the placement of sensor arrays over strategic locations [4].

Recent advances in the field of flexible electronics have resulted in increased interest in the use of dense sensor networks (DSNs) to solve the local-global monitoring challenge [1, 9] . These networks, often termed electronic artificial skins, e-skins, or sensing skins are thin electronic sheets that mimic the sensing ability of biological skin.

Electronic skins often consist of rigid or semi-rigid cells mounted on a flexible sheet. Lee *et al.* developed and demonstrated an artificial skin sensor capable of localizing physical interactions through a flexible capacitive tactile sensor. Experimentally verified using a 16 x 16 array of cells, this artificial skin provided a spatial resolution of 1 mm [10]. Shear stress topography and flow separation on the leading edge of a delta-wing structure during wind tunnel tests was recently measured using a sensing skin consisting of a 36-sensor array of resistive heating elements on a flexible polyimide film [11]. Recently, research has progressed towards the devolvement of microelectromechanical systems (MEMS) mounted onto flexible polymer skins without the need for ridged packaging [12, 13].

Deployment of DSNs capable of covering mesoscale systems have also been proposed. Termed large area electronics (LAE), these integrated sensing skins enable direct sensing and can be scaled for the monitoring of mesoscale systems. Yao *et al.* developed a strain sensing sheet for crack detection and localization, based on resistive strain gauges (RSGs). The LAE is capable of detecting cracks (i.e., local condition monitoring) and producing full field strain maps (i.e., global condition monitoring) [14]. Additionally, the use of resistance-based thin-film strain sensors fabricated with carbon nanotubes has attracted considerable attention. Thin film resistance-based sensors offer potential scalability. Examples of such sensors include a strain sensor fabricated from single-walled carbon nanotubes (SWCNT) exhibiting a relatively high gauge factor of 5 [15]. Burton *et al*. demonstrated an integrated CNT-polymer composite deployed onto a flexible polyimide substrate with its associated electronics. A strain resolution of 50με and a gauge factor of 0.77 were experimentally verified [16].

Capacitive-based sensing skins have also been studied for monitoring strain [17], pressure [18], triaxial force [19], and humidity [20]. Within the same framework of LEAs described above, the authors have developed a soft elastomeric capacitor (SEC) suitable for use in the monitoring of mesoscale systems. The proposed SEC is inexpensive and offers a simple manufacturing process. The SEC was developed around an inexpensive nanocomposite based on a styrene-co-ethylene-co-butylene-co-styrene (SEBS) block co-polymer matrix filled with titania for the dielectric and carbon black for the electrodes. The SEC is customizable in shape [21, 22], and its static [22] and dynamic behaviors [23, 1] have been characterized, including damage detection applications in wind turbine blades [24] subjected to random wind loadings [25]. The effectiveness of a DSN consisting of SECs for detecting fatigue cracks has been demonstrated [26].

A particular feature of the SEC is its ability to measures additive in-plane strain. When deployed in a DSN configuration, the SEC is able to monitor local additive strain over large areas. The sensors' signals can be used to decompose additive strain maps into linear strain components along two orthogonal directions provided certain boundary conditions are known. The authors presented an algorithm in [27] designed to leverage a DSN configuration to enable strain field decomposition. The algorithm fits linear strain components with a prescribed shape function assuming the validity of the classical Kirchhoff plate theory, and the coefficients of the shape function can be computed using a least squares estimator (LSE). This work was further enhanced through the introduction of RSGs into the DSN to form a hybrid dense sensor network (HDSN) were the RSGs are used to enforce the algorithm's boundary conditions [28]. Numerical simulations and experimental results showed promise of the algorithm.

In this paper, the use of an HDSN consisting of an array of SECs and RGSs is experimentally verified for damage detection and localization on a model wind turbine blade. The HDSN is installed inside a wind turbine blade model and tested in a wind tunnel to simulate an operational environment. The paper is organized as follows. First, the background on the SEC sensor in introduced, along with the strain decomposition algorithm. Second, the test methodology for the experimental validation is presented, which includes the algorithm formulation specialized for the model wind turbine blade. Third, a validation of the HDSN's capability to detect, localize and quantity damage is presented. Finally, a summary of the results concludes the paper.

BACKGROUND

The SEC provides direct capacitance to strain signal. The electromechanical model mapping a change in the SEC capacitance ΔC to a change in its strain is written [28]

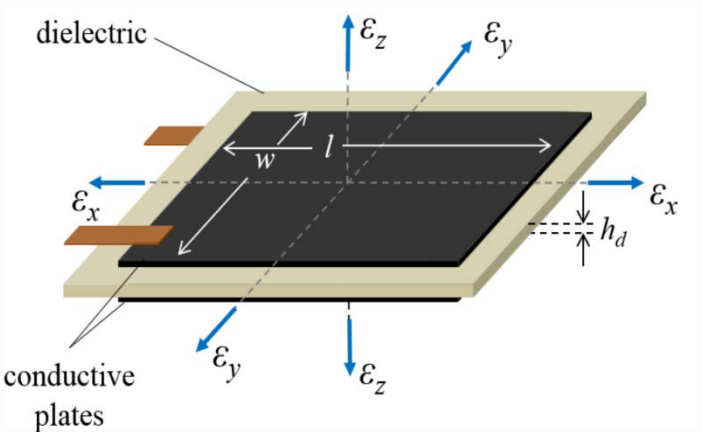

Figure 1. Schematic representation of an SEC

$$\frac{\Delta C}{C_0} = \frac{1}{1-\nu}(\varepsilon_x + \varepsilon_y) \tag{1}$$

$$C_0 = e_0 e_r A / h_d \tag{2}$$

where ε_x and ε_y are the in-plane strains as shown in fig. 1, $\nu \approx 0.49$ is the Poisson ratio of the polymer, e_0 is the vacuum permittivity, e_r is the polymer relative permittivity, $A = w \cdot l$ is the initial sensor area of initial width w and length l, and h_d is the initial height of the dielectric. The gauge factor λ can be approximated as $\lambda = 1/(1-\nu) \approx 2$. This formulation assumes that the material is incompressible and under plane stress ($\sigma_z = 0$).

Strain Decomposition Algorithm

As discussed above, the SEC signal comprises the additive in-plane strain components. The algorithm for surface strain reconstruction proposed by Wu *et al.* consists of assuming a shape function, enforcing the boundary conditions, and computing the coefficients of the shape function using an LSE [27]. Downey *et al.* presented an enhanced LSE strain decomposition algorithm where RSGs are used to directly measure boundary conditions within a network of SEC sensors. The combination of RSGs with an SEC network formed an HDSN [28]. Additionally, the enhanced strain decomposition algorithm introduced virtual sensor nodes at key locations where strain is known, or can be assumed within a relatively high degree of certainty.

The enhanced LSE algorithm is diagramed in fig. 2, and derived in [27] and [28]. Briefly, the algorithm consists of assuming a parametric displacement shape function. For simplicity consider a cantilever plate in the *x*-*y* plane with a thickness *c*, and fixed along one edge ($x = 0$). An n^{th} order polynomial is selected due to its mathematical simplicity to approximate the plate's deflection shape. The deflection shape $w_{(x,y)}$ is expressed as

$$w_{(x,y)} = \sum_{i=1,j=0}^{n} b_{ij} x^i y^i \tag{3}$$

where b_{ij} are regression coefficients, with $i > 0$ to satisfy the displacement boundary condition on the clamped edge ($w_{(0,y)} = 0$). Considering a network with *m* sensors and collecting displacements at sensors' locations in a vector **W**, equation (3) can be written

$$\mathbf{W} = [w_1 \dots w_k \dots w_m]^T = \mathbf{HB} \tag{4}$$

where **H** encodes the sensor location information and **B** is the regression coefficients matrix. The **H** matrix is developed from quantities contained in equation (3)

$$\mathbf{H} = \left[\mathbf{H}_x | \mathbf{H}_y\right] = \begin{bmatrix} w_{(x,y),1} & w_{(x,y),1} \\ \vdots & \vdots \\ w_{(x,y),m} & w_{(x,y),m} \end{bmatrix} \tag{5}$$

$$\mathbf{B} = \left[\mathbf{H}_x \mid \mathbf{H}_y\right] = \left[\beta_{10} \dots \beta_{ij} \dots \beta_{nm}\right] \tag{6}$$

where $\mathbf{H}_x$, $\mathbf{H}_y$, $\mathbf{B}_x$ and $\mathbf{B}_y$ are subsets of **H** and **B**, respectively. Linear strain functions ε_x and ε_y along the *x* and *y* directions, respectively, can be obtained from equation (3) assuming Kirchhoff's plate theory as:

$$\varepsilon_x = \frac{c}{2} \frac{\partial^2 \boldsymbol{W}}{\partial x^2} = \boldsymbol{H}_x \mathbf{B}_x \tag{7}$$

$$\varepsilon_y = \frac{c}{2} \frac{\partial^2 \boldsymbol{W}}{\partial y^2} = \mathbf{H}_y \mathbf{B}_y \tag{8}$$

and written in terms of sensors' signals;

$$\mathbf{S} = [s_1 \dots s_k \dots s_m]^T = \varepsilon_x + \varepsilon_y = \mathbf{H}_s \mathbf{A}_s \tag{9}$$

where s_k is expressed as;

$$s_k = \frac{\Delta C_k}{\lambda C_k} = \varepsilon_{x,k} + \varepsilon_{y,k} \tag{10}$$

as derived in equation (1). Lastly, the regression coefficient matrix B is estimated using the least squares estimator;

$$\widehat{\mathbf{B}} = (\mathbf{H}^{\mathrm{T}}\mathbf{H})^{-1}\mathbf{HS} \tag{11}$$

where the hat denotes an estimation. In its unaltered form, **H** is multi-collinear because $\mathbf{H}_x$ and $\mathbf{H}_y$ share multiple columns, and $\mathbf{H}^{\mathrm{T}}\mathbf{H}$ is therefore singular and non-invertible. To obtain a full rank $\mathbf{H}^{\mathrm{T}}\mathbf{H}$, boundary conditions on the strain map need to be included within **H**. This is done through the introduction of RSG sensors into the **H** matrix. The RSG signal is assumed to be unidirectional. Therefore, an RSG sensor *k* is added into $\mathbf{H}_{x,k}$ or $\mathbf{H}_{y,k}$ determined by the RSG orientation and nullifying the corresponding row in $\mathbf{H}_{x,k}$ or $\mathbf{H}_{y,k}$. Due to the high level of precision typically provided by RSGs, a higher weight can be applied in the LSE at their respective locations, $\mathbf{H}_{x,k}$ or $\mathbf{H}_{y,k}$. Finally, virtual sensor nodes are added into the **H** matrix simulating RSG sensors at locations of know strain, i.e. along boundary conditions.

METHODOLOGY

An HDSN consisting of 12 SECs and 8 RSGs was deployed onto the inside surface of a model wind turbine blade. The experimental setup is shown in fig. 3, consisting of a 1.3 meter blade modeled after the center third of a full scale wind turbine blade. The model (fig. 3(a)) consisted of 10 airfoil sections mounted onto an aluminum spar. A fiberglass composite skin was attached to the second and third airfoil sections counted from the blade root. Damage was induced into the fiberglass composite skin in the form of a cut, shown in fig. 3(b), to simulate a surface crack in the blade. Various damage cases were induced into the fiberglass substrate by cutting along the horizontal line in fig. 3(b), from the center outwards. A damage case of 2 cm is shown in fig. 3(b). Data was collected for the undamaged condition,

as well as from crack lengths varying from 2 cm to 13 cm, in 1 cm step increment. The induced cut is 2 mm wide and goes completely through the fiberglass substrate.

This setup provided an experimental platform for the validations of an HDSN in a simulated wind turbine environment. The model was mounted vertically with the blade root up in the Aerodynamic and Atmospheric Boundary Layer (AABL) wind and gust tunnel located in the Wind Simulation and Testing Laboratory (WiST Lab) in the Department of Aerospace Engineering at Iowa State University. The wind tunnel has an aerodynamic test section of 2.44 m width by 1.83 m height, an atmospheric boundary layer test section of 2.44 m width by 2.21 m height, and a design maximum wind speed of 53 m/s in the aerodynamic test section. Vibrations were induced by forcing two parallel thin-plates (with rounded edges at a fixed spacing), mounted vertically upstream of the model, to oscillate at a characteristic frequency of 3.1 Hz, thereby creating a sinusoidal buffeting (turbulence-induced) load (lift and moment) along the span of the blade. The blade root was restrained in all 6 degrees-of-freedom, while forces at the root were monitored via force transducers. Two Transducer Techniques model MDB-50 were used to monitor lift and moment, and a MDB-25 was used to measure drag forces at the root. Lastly, the model was instrumented with 7 accelerometers, PCB model #352C65 , mounted on the inside of the model.

The HDSN implemented for this test consisted of 12 3x3cm square SECs and 8 unidirectional RSGs, TML model #FCA-2. The sensor layout is illustrated in fig. 4(a). Figure 4(b) is a picture of the fiberglass panel that was attached to the blade model with 12 SECs and 4 of the 8 RSGs mounted. The remaining 4 RSGs were added after the panel was attached to the model. The SEC data acquisition consisted of three custom built microcontrollers, Atmel P328, each with a 24 bit 4 channel capacitance to digital (CDC) convertor. RSG measurements were recorded using a National Instruments 24-bit 350 Ω quarter-bridge modules (NI-9236). SEC and RSG data were collected using LabVIEW and sampled at 22 and 2000 Hz, respectively.

Interference between the SEC data acquisition microcontrollers required that only one microcontroller be operating at any given time. Therefore, experimental data was obtained over 3 individual test runs, each test recording 4 SECs and all eight RSGs. Final experimental data were compiled using the RSG signal as a reference to obtain the SEC signals for each damage case. Sensor signals were filtered as follows. First, a low pass Weibull filter with a cutoff frequency of 5 Hz was implemented on both the SEC and RSG signals. Second, a principal component analysis (PCA) decomposition was applied on the SEC signals, retaining the first four eigenvalues. The SEC signal was then resampled to 100 Hz using a spline interpolation. Third, the RSG signal synchronized with the 100 Hz SEC signal, resulting in the common time stamp needed for the implementation of the enhanced LSE algorithm.

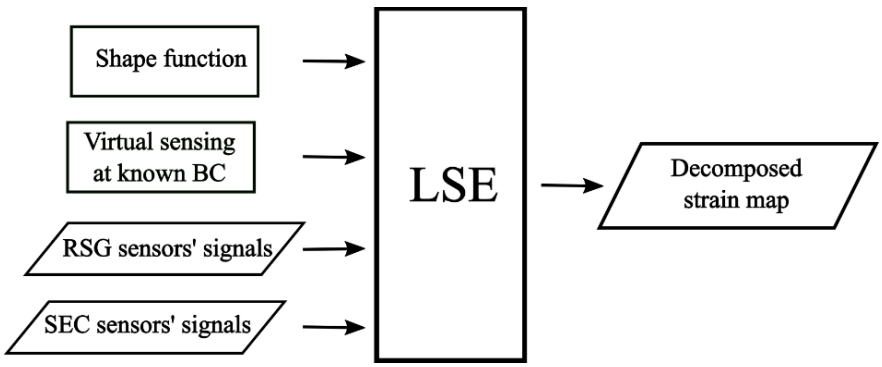

Figure 2. LSE strain reconstruction algorithm

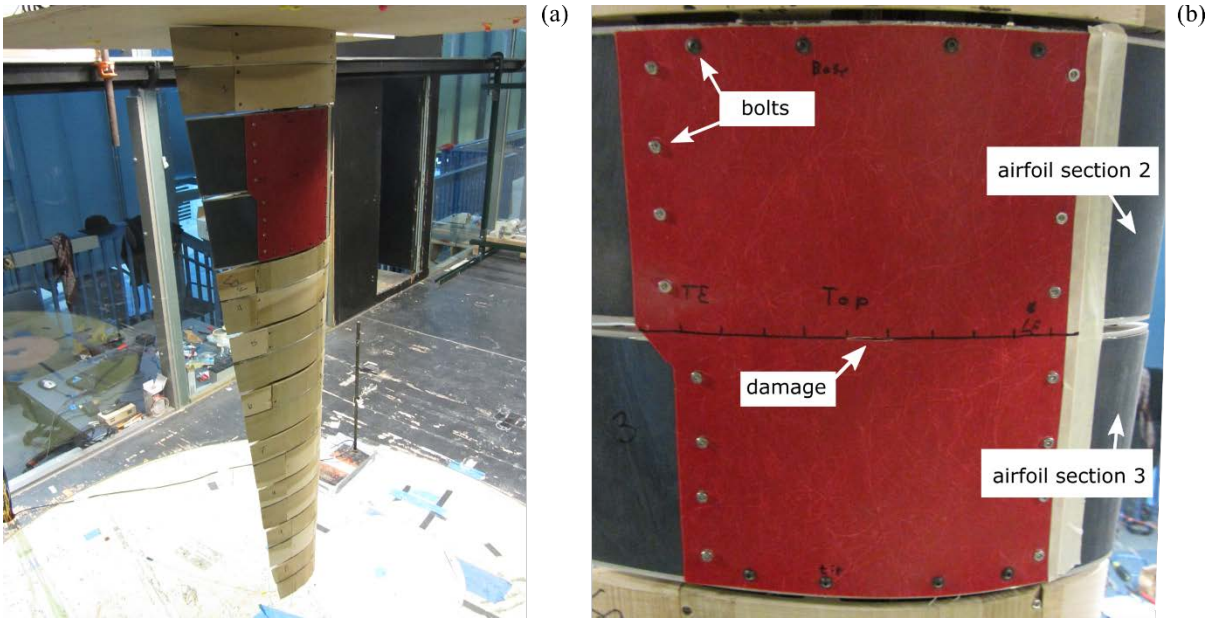

Figure 3. Experimental setup: (a) wind turbine blade mounted in wind tunnel; and (b) composite section, with a crack length of 2 cm, mounted on the model.

Algorithm Properties

A sixth order polynomial function (Eq. 3) for the deflection shape was selected to improve the ability of the strain decomposition algorithm in capturing the complex strain features present in the experimental test while still requiring low computational time. A displacement field (**W**) was constructed such that

$$w_{(x,y)} = \sum_{i=1,j=0}^{6} b_{ij} x^i y^i \tag{12}$$

All eight RSGs were used to enforce boundary conditions within the HDSN. RSGs were introduced into the **H** matrix as unidirectional sensors. A unity weight was applied to the RSGs in the current formulation. Therefore, the LSE algorithm uses equal weights for both the RSG and SEC data when fitting the reconstructed strain maps.

Virtual sensing nodes were deployed where strain in principal directions is known or can be assumed with a high level of accuracy to be zero. These positions are diagramed in fig. 4(a) with blue squares representing boundary conditions where is $\varepsilon_x = 0$, and red circles represent locations where the condition $\varepsilon_y = 0$. Virtual sensors were not placed at corners to allow for the presence of high concentrations of strain in the reconstructed strain maps.

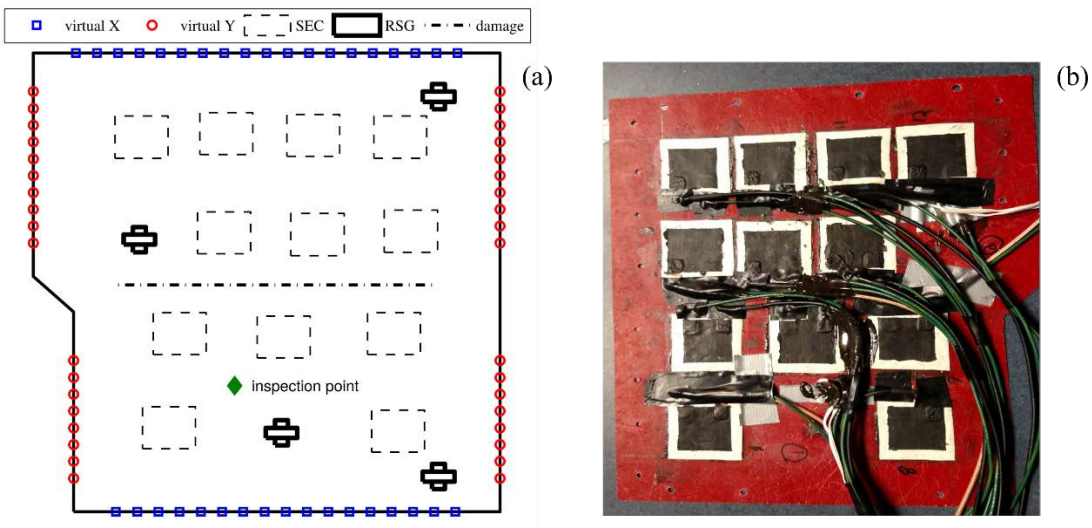

Figure 4. Experimental HDSN configuration: (a) schematic, where dashed squares represent SECs and crosses represent two RSGs measuring strain in orthogonal directions; virtual sensors in the *x* and *y* directions are denoted with blue squares red circles, respectively; and (b) picture of the HDSN (RSGs under wires) view from inside the blade model.

VALIDATION

The ability of the HDSN to function as a sensing skin capable of detecting, localizing, and quantifying damage is validated. Figure 5 shows the decomposed strain maps ($\mu\varepsilon_x$ and $\mu\varepsilon_y$) for the healthy and three individual damage cases (2 cm, 8 cm and 18 cm). Each strain map is computed from data taken when the strain is at its maximum i.e. when the tip of the model is at its maximum displacement. The reconstructed decomposed strain maps for the undamaged test case are presented in fig. 5(a). As expected, the majority of the strain energy is present in the middle of the fiberglass skin that connects the two separate airfoil sections. The deployed HDSN is capable of

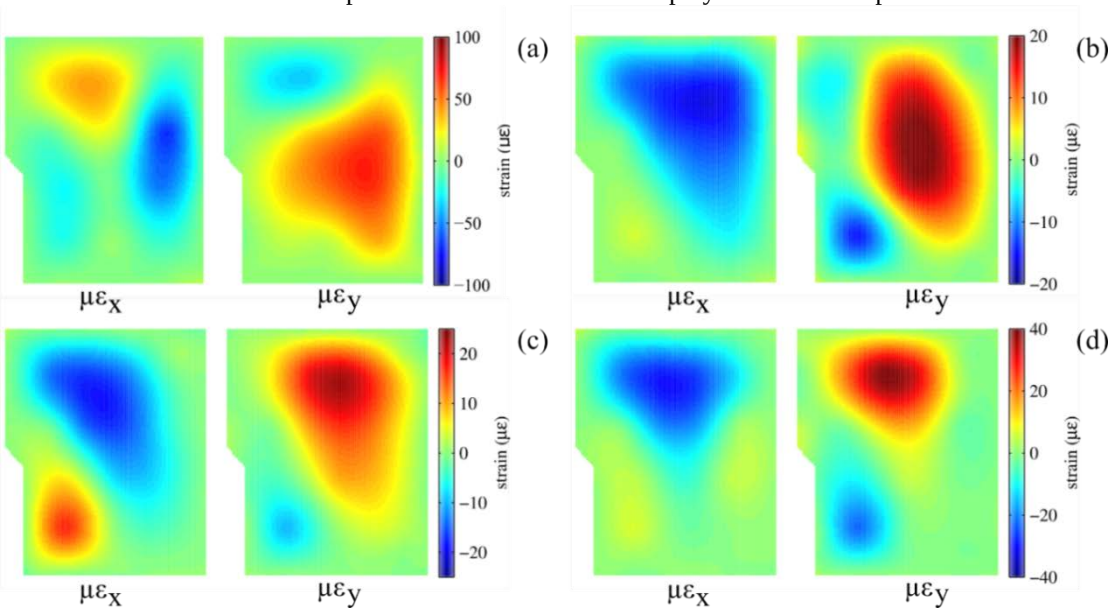

Figure 5. Reconstructed strain maps με*x* and με*y*: (a) healthy skin condition; (b) 2 cm cut; (c) 8 cm cut; and (d) 13 cm cut, damage maps are relative to the undamaged strain maps.

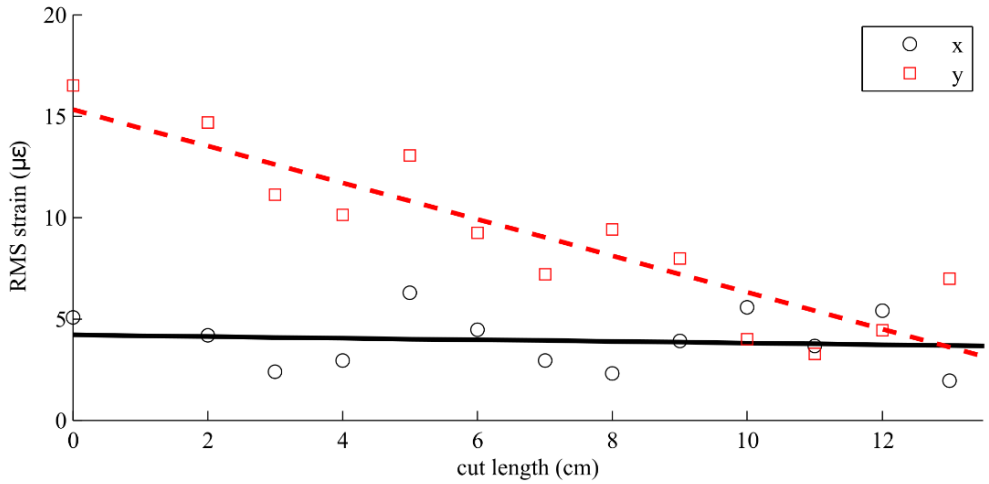

Figure 6. Reconstructed strain maps με*x* and με*y*: (a) healthy skin condition; (b) 2 cm cut; (c) 8 cm cut; and (d) 13 cm cut.

reconstructing the relatively complex strain fields such as the torsional motion of the blade model as represented by the different parts of the skin being under tension and compression. The blades' torsion detected by the strain maps was corroborated through accelerometers, force transducers, and video captured during experimental testing.

The comparison of strain maps across different damage cases (fig. 5(b)-(d)) enables the detection of damage through a change in the strain flow, where the location of maximum strain shifting away from the center of the fiberglass sheet as the crack grows in length.

An advantage of the HDSN combined with the enhanced LSE algorithm is the capability to estimate strain over the entire monitored component, which data can be used for condition assessment. For example, fig. 6 shows the evolution of the estimated strain at the "inspection point", depicted in fig. 4(a), situated close to the induced damage. Data is presented as the root mean square (RMS) value of strain time history. The evolution of the RMS as a function of the cut length at that particular point shows a linearly decreasing strain in the *y*-direction, while the strain in the *x*-direction is approximately constant. The RMS value at that point gives a quantitative measure of damage. It is thus possible to utilize the HDSN for damage diagnosis, localization, and quantification.

CONCLUSION

This paper presented a novel hybrid dense sensor network (HDSN) sensing strategy for monitoring of strain over large surfaces. The HDSN was tested on a scale model of a wind turbine blade in a wind tunnel to simulate an operational environment. The HDSN consisted of a novel skin-type sensor based on a soft elastomeric capacitor combined with resistive strain gauges (RSGs), an off-the-shelf sensing technology. An enhanced least squares estimator (LSE)-based algorithm was used to decompose additive strain measurements into unidirectional strain maps. The algorithm assumed a shape function, enforced boundary conditions with RSG measurements and virtual sensors, and computed regression coefficients using an LSE.

Experimental results demonstrated the ability to the HDSN to detect changes in strain maps (i.e. damage) resulting from damage that provoked a change in load path. Damage quantification was also made possible by investigating the change in the root mean square value of strain at a particular point that was known to be located close to the induced damage. These results showed the promise of the HDSN technology at monitoring very large structural components. Also, given the ability of the HDSN at measuring strain maps, the technology could be used to update physical models

in real-time, therefore creating high fidelity models that can be used for further research and development on the component itself, or the design of highly effective structural health monitoring strategies through the discovery of hot spots.

ACKNOWLEDGMENTS

The development of the SEC technology was supported by grant No. 13-02 from the Iowa Energy Center. This work is also partly supported by the National Science Foundation Grant No. 1069283, which supports the activities of the Integrative Graduate Education and Research Traineeship (IGERT) in Wind Energy Science, Engineering and Policy (WESEP) at Iowa State University. Their support is gratefully acknowledged.

REFERENCES

[1] S. Laflamme, F. Ubertini, H. Saleem, A. D'Alessandro, A. Downey, H. Ceylan and A. L. Materazzi, "Dynamic Characterization of a Soft Elastomeric Capacitor for Structural Health Monitoring," *Journal of Structural Engineering*, vol. 141, no. 8, p. 04014186, 2015.

[2] P. C. Chang, A. Flatau and S. C. Liu, "Review Paper: Health Monitoring of Civil Infrastructure," *Structural Health Monitoring*, vol. 2, no. 3, pp. 257-267, 2003.

[3] D. Adams, J. White, M. Rumsey and C. Farrar, "Structural health monitoring of wind turbines: method and application to a HAWT," *Wind Energy*, vol. 14, no. 4, pp. 603-623, 2011.

[4] C. C. Ciang, J.-R. Lee and H.-J. Bang, "Structural health monitoring for a wind turbine system: a review of damage detection methods," *Measurement Science and Technology*, vol. 19, no. 12, p. 122001, 2008.

[5] F. Ubertini, A. L. Materazzi, A. D'Alessandro and S. Laflamme, "Natural frequencies identification of a reinforced concrete beam using carbon nanotube cement-based sensors," *Engineering structures*, vol. 60, pp. 265-275, 2014.

[6] Y. Zou, L. P. S. G. Tong and G. P. Steven, "Vibration-based model-dependent damage (delamination) identification and health monitoring for composite structures—a review," *Journal of Sound and vibration*, vol. 230, no. 2, pp. 357-378, 2000.

[7] E. Gross, T. Simmermacher, M. Rumsey and R. I. Zadoks, "Application of damage detection techniques using wind turbine modal data," in *American Society of Mechanical Engineers Wind Energy Symp.(Reno, NV, USA)*, 1999.

[8] M. A. Rumsey and J. A. Paquette, "Structural health monitoring of wind turbine blades," in *The 15th International Symposium on: Smart Structures and Materials \& Nondestructive Evaluation and Health Monitoring*, 2008.

[9] J. A. Rogers, T. Someya and Y. Huang, "Materials and mechanics for stretchable electronics," *Science*, vol. 327, no. 5973, pp. 1603-1607, 2010.

[10] H.-K. Lee, S.-I. Chang and E. Yoon, "A flexible polymer tactile sensor: fabrication and modular expandability for large area deployment," *Microelectromechanical Systems, Journal of*, vol. 15, no. 6, pp. 1681-1686, 2006.

[11] Y. Xu, F. Jiang, S. Newbern, A. Huang, C.-M. Ho and Y.-C. Tai, "Flexible shear-stress sensor skin and its application to unmanned aerial vehicles," *Sensors and Actuators A: Physical*, vol. 105, no. 3, pp. 321-329, 2003.

[12] M. S. Mahmood, Z. Celik-Butler and D. P. Butler, "Design and fabrication of self-packaged, flexible MEMS accelerometer," in *SENSORS, 2015 IEEE*, 2015.

[13] M. Ahmed, I. E. Gonenli, G. S. Nadvi, R. Kilaru, D. P. Butler and Z. Celik-Butler, "MEMS sensors on flexible substrates towards a smart skin," in *Sensors, 2012 IEEE*, 2012.

[14] Y. Yao and B. Glisic, "Detection of steel fatigue cracks with strain sensing sheets based on large area electronics," *Sensors*, vol. 15, no. 4, pp. 8088-8108, 2015.

[15] I. Kang, M. J. Schulz, J. H. Kim, V. Shanov and D. Shi, "A carbon nanotube strain sensor for structural health monitoring," *Smart Materials and Structures,* vol. 15, no. 3, p. 737, 2006.

[16] A. R. Burton, M. Kurata, H. Nishino and J. P. Lynch, "Fully integrated patterned carbon nanotube strain sensors on flexible sensing skin substrates for structural health monitoring," in *SPIE Smart Structures and Materials+ Nondestructive Evaluation and Health Monitoring*, 2016.

[17] M. Suster, J. Guo, N. Chaimanonart, W. H. Ko and D. J. Young, "A high-performance MEMS capacitive strain sensing system," *Microelectromechanical Systems, Journal of,* vol. 15, no. 5, pp. 1069-1077, 2006.

[18] D. J. Lipomi, M. Vosgueritchian, B. C. K. Tee, S. L. Hellstrom, J. A. Lee, C. H. Fox and Z. Bao, "Skin-like pressure and strain sensors based on transparent elastic films of carbon nanotubes," *Nature Nanotechnology,* vol. 6, no. 12, pp. 788-792, 2011.

[19] J. A. Dobrzynska and M. A. M. Gijs, "Polymer-based flexible capacitive sensor for three-axial force measurements," *Journal of Micromechanics and Microengineering,* vol. 23, no. 1, p. 015009, 2012.

[20] P. M. Harrey, B. J. Ramsey, P. S. A. Evans and D. J. Harrison, "Capacitive-type humidity sensors fabricated using the offset lithographic printing process," *Sensors and Actuators B: Chemical,* vol. 87, no. 2, pp. 226-232, 2002.

[21] S. Laflamme, M. Kollosche, J. J. Connor and G. Kofod, "Robust Flexible Capacitive Surface Sensor for Structural Health Monitoring Applications," *Journal of Engineering Mechanics,* 2012.

[22] S. Laflamme, H. S. Saleem, B. K. Vasan, R. L. Geiger, D. Chen, M. R. Kessler and K. Rajan, "Soft Elastomeric Capacitor Network for Strain Sensing Over Large Surfaces," *Mechatronics, IEEE/ASME Transactions on,* vol. 18, no. 6, pp. 1647-1654, Dec 2013.

[23] H. Saleem, A. Downey, S. Laflamme, M. Kollosche and F. Ubertini, "Investigation of Dynamic Properties of a Novel Capacitive-based Sensing Skin for Nondestructive Testing," *Materials Evaluation,* vol. 73, no. 10, pp. 1390-1397, 2015.

[24] S. Laflamme, L. Cao, E. Chatzi and F. Ubertini, "Damage Detection and Localization from Dense Network of Strain Sensors," *Shock and Vibration,* vol. 2016, no. 2562949, pp. 1-13, 2016.

[25] F. Ubertini and F. Giuliano, "Computer Simulation of Stochastic Wind Velocity Fields for Structural Response Analysis: Comparisons and Applications," *Advances in Civil Engineering,* vol. 2010, no. 749578, pp. 1-20, 2010.

[26] S. Kharroub, S. Laflamme, C. Song, D. Qiao, B. Phares and J. Li, "Smart sensing skin for detection and localization of fatigue cracks," *Smart Materials and Structures,* vol. 24, no. 6, p. 065004, 2015.

[27] J. Wu, C. Song, H. S. Saleem, A. Downey and S. Laflamme, "Network of flexible capacitive strain gauges for the reconstruction of surface strain," *Measurement Science and Technology,* vol. 26, no. 5, p. 055103, 2015.

[28] A. Downey, S. Laflamme and F. Ubertini, "Distributed thin film sensor array for damage detection and localization," in *SPIE Smart Structures and Materials+ Nondestructive Evaluation and Health Monitoring*, 2016.

[29] D. M. Frangopol and T. B. Messervey, "Life-cycle cost and performance prediction: role of structural health monitoring," *Frontier technologies for infrastructures engineering: structures and infrastructures book series,* vol. 4, p. 361, 2009.